Hepatic Glucagon-receptor Signaling Enhances Insulin-Stimulated Glucose Disposal in Rodents

[1]Teayoun Kim, [1]Cassie L. Holleman, [1]Shelly Nason, [2]Deanna M Arble, [3]Nickki Ottaway, [4]Joseph Chabenne, [1]Christine Loyd, [1]Jeong-a Kim, [5]Darleen Sandoval, [6]Daniel J. Drucker, [4,7]Richard DiMarchi, [3]Diego Perez-Tilve[#], & [1]Kirk M Habegger[#]

[1]Comprehensive Diabetes Center and Department of Medicine – Division of Endocrinology, Diabetes and Metabolism, University of Alabama at Birmingham, Birmingham, AL USA
[2] Department of Biological Sciences, Marquette University, Milwaukee, WI, USA
[3]Metabolic Disease Institute, Division of Endocrinology, Diabetes and Metabolism, Department of Medicine, University of Cincinnati, Cincinnati OH, USA
[4] Novo Nordisk Research Center, 5225 Exploration Drive, Indianapolis, IN 46241, USA.
[5]Department of Surgery, University of Michigan, Ann Arbor, MI, USA
[6]Lunenfeld-Tanenbaum Research Institute, Mt. Sinai Hospital, Department of Medicine, University of Toronto, Toronto, ON, CA
[7]Department of Chemistry, Indiana University, Bloomington, IN, USA

[#] Correspondence to:
Kirk M Habegger - Lead Contact
Department of Medicine - Endocrinology, Diabetes & Metabolism
University of Alabama at Birmingham
Birmingham, AL 35294
Email - kirkhabegger@uabmc.edu

Diego Perez-Tilve
Metabolic Disease Institute, Division of Endocrinology, Diabetes & Metabolism,
Department of Internal Medicine, College of Medicine,
University of Cincinnati,
Cincinnati, OH 45230
Email - pereztdo@ucmail.uc.edu

Key words:
Glucagon
Glucose tolerance
Insulin Action
Insulin Signaling
AKT
Insulin Sensitivity

Abstract

Glucagon receptor (GCGR) agonists cause hyperglycemia but also weight loss. However, GLP1R/GCGR mixed agonists do not exhibit the diabetogenic effects often attributed to GCGR activity. Thus, we sought to investigate the effect of glucagon agonism on insulin action and glucose homeostasis. Acute GCGR agonism induced immediate hyperglycemia, followed by improved glucose tolerance and enhanced glucose-stimulated insulin secretion. Moreover, acute GCGR agonism improved insulin tolerance in a dose-dependent manner in both lean and obese mice. Improved insulin tolerance was independent of GLP1R, FGF21, and hepatic glycogenolysis. Moreover, we observed increased glucose infusion rate, disposal, uptake, and suppressed endogenous glucose production during euglycemic clamps. Mice treated with insulin and GCGR agonist had enhanced phosphorylation of hepatic AKT at Ser^{473}; this effect was reproduced in isolated mouse primary hepatocytes and resulted in increased AKT kinase activity. These data reveal that GCGR agonism enhances glucose tolerance in part, by augmenting insulin action, with implications for the use of GCGR agonism in therapeutic strategies for diabetes.

Introduction

Glucagon (GCG) is a 29-amino acid peptide released from a-cells of the pancreatic islet. Its role as a primary counterregulatory hormone to insulin action has long received scientific attention, yet its broader therapeutic potential is underappreciated(1; 2). Intriguingly, the antidiabetic actions of glucagon-like peptide-1 receptor (GLP1R) agonism are enhanced by the catabolic and hypolipidemic properties of glucagon receptor (GCGR) agonism(3-5). Importantly, GLP1R/GCGR mixed agonists do not exhibit the hyperglycemia and glucose intolerance often attributed to GCGR activity; findings that were confirmed in human subjects(6). Moreover, postprandial elevations of glucagon and GLP1 may contribute to improved postprandial glucose homeostasis in Roux-en-Y gastric bypass patients(7; 8). How GCGR mono-agonism promotes transient glucose intolerance, yet simultaneously contributes to the anti-diabetic actions of incretin-based therapies is still unknown. As a counterregulatory hormone with a role in maintaining fasting blood glucose, it is tempting to assume that glucagon opposes all actions of insulin. However, the increased concentrations and action of glucagon in the fasting state are well suited to potentiate subsequent, insulin-mediated glucose control. In the context of normal physiology, exercise induces glucagon secretion(9) and modulates the cephalic response of meal assimilation(10). Altogether these data suggest that glucagon may in fact contribute to these states of heightened insulin sensitivity.

Chronic GCGR agonism in diet-induced obese (DIO) mice stimulates weight loss, hyperglycemia, and glucose intolerance(11). Unexpectedly, GCGR signaling

in *db/db* mice improved the rate of insulin-stimulated glucose disappearance (k_g)(11). Here we demonstrate that, in addition to its counterregulatory role, hepatic GCGR agonism enhances systemic insulin-stimulated glucose disposal. Together, this data mechanistically elucidates how glucose control may be improved by therapies characterized by glucagon agonism.

Materials & Methods

Animal models. All studies were approved by and performed according to the guidelines of the Institutional Animal Care and Use Committee of the University of Alabama at Birmingham or the University of Cincinnati. Mice were single or group-housed on a 12:12-h light-dark cycle (light on from 0600 to 1800 h) at 22°C and constant humidity with free access to food and water, except as noted. *Fgf21*-, *Gcgr* floxed, and *Glp1r*-deficient mice were generated as previously described (12-15) and *Alb*-Cre mice obtained from Jackson Labs (Bar Harbor, ME). All mice were maintained in our facilities on a C57Bl/6J background and fed a standard chow (Teklad LM-485, 5.6% fat) or high fat diet (HFD, 58.0 kcal% fat; D12331 Research Diets, New Brunswick NJ).

Peptides and inhibitors. Novel GCGR agonists (IUB288 and ASP28,GLU29-glucagon) were synthesized as previously described (11; 16). Native glucagon and insulin (Humulin® R) were obtained from American Peptide Co. and Eli Lilly and Co., respectively. Glycogen phosphorylase a/b inhibitor, BAY R3401, was obtained from Sigma-Aldrich and diluted in 0.5%methyl cellulose.

Glucose and insulin tolerance tests. Glucose and insulin tolerance tests (GTT, ITT) were performed in 6-h fasted 8-10 week-old chow-fed, or 24 week-old diet-induced obese, male C57Bl/6J mice by ip injection of IUB288 (10 nmol/kg) or glucagon (10 nmol/kg) 60 min prior to ip injection of glucose (2 g/kg, 20% wt/vol D-glucose [Sigma] in 0.9% wt/vol saline) or insulin (0.25 – 1.0 unit/kg in 0.9%

wt/vol saline). ITTs were conducted in lean, chow-fed, male *Glp1r*$^{-/-}$ and *Fgf21*$^{\Delta liver}$ mice at 10-14 weeks old. GTT and ITT were conducted in 8-12 and 10-14 week/old *Gcgr*$^{\Delta liver}$ mice, respectively. Blood glucose was determined by TheraSense Freestyle Glucometer. Glucose disappearance rate (k_g) was defined as ($^{\Delta \text{ blood glucose}}/_{\text{minute}}$). Insulin and C-peptide were measured from blood collected 60 min after IUB288 challenge.

i.v. Glucose-stimulated insulin secretion (GSIS) and GCGR agonist infusion tests. Catheters were surgically implanted as previously described (17). Four days after surgery, lean, chow-fed, 14-week-old, male C57Bl/6J mice were fasted 5 h. IUB288 injection (10 nmol/kg ip) was administered 60 min prior to glucose bolus (1 g/kg) delivered via venous catheter. Plasma samples collected immediately before and 2, 5, 10, and 15 min after infusion. For GCGR agonist infusion studies chow-fed, 14 week old, male C57Bl/6J mice were fasted for 4 h before 120 min Asp28,Glu29-glucagon infusion (0.00064 and 0.0064 nmol/min). Mice were administered 0.25 U/kg insulin ip and euthanized 20 min later.

Euglycemic-Clamps. Clamps conducted as previously described (17). Briefly, catheters were implanted in male 8 w old, chow-fed, C57Bl/6J mice. Four to six days post-op, mice were fasted 5h with saline or IUB288 (10 nmol/kg) injected (s.c.) during the final 60 min. Insulin (4mU/kg/min, diluted in saline) was infused through the venous catheter and euglycemia (140 mg/dL) was maintained by adjusting the infusion rate of a 20% glucose solution. A tracer equilibration period

(t = -120 to 0 min) was utilized as follows: a 5 μCi bolus of [3-^{3}H]-Glucose (Perkin Elmer, Boston, MA) was given at t = -120 min followed by a 0.05 μCi/min infusion for 2 hr. Somatostatin (SST; EMD Millipore, Temecula, CA), mixed with the [3-^{3}H]-Glucose, was infused at 1.5 μg/kg/min from t = -120 to 0 min and at 3 μg/kg/min from t = 0 min to 120 min. At t=0 [3-^{3}H]-Glucose infusion was increased to 0.1 μCi/min to minimize changes in specific activity (SA). The variation of SA was less than 10% from mean during the last 40min of clamp, and the slope of SA over time was not significantly different from t = 0. Blood samples (100 μl) were taken at -120, -60, -30, -5, 90, 100, 110, and 120 min for the assessment of glucose, insulin, and glucose SA in plasma. Red blood cells from these samples were recovered by centrifugation and injected via arterial catheter to prevent a hematocrit deficit. A 10 μCi, [1-^{14}C]-2 deoxy-D-glucose (2DG) (MP Biomedicals, Santa Ana, CA) bolus was injected at t = 75 min via carotid arterial catheter to assess glucose uptake. Following the clamp, mice were euthanized and tissues (gastrocnemius, soleus, extensor digitorum longus (EDL), quadriceps, liver, gonadal white adipose tissue (WAT), and interscapular brown adipose (BAT)) were snap frozen in liquid nitrogen.

Biochemical Assays

Plasma [3-^{3}H]-Glucose, [1-^{14}C]-2DG, and $^{3}H_2O$ were measured to determine Ra, Rd, and uptake as previously described(17). Clamp plasma glucose was measured from 20 μl of deproteinized samples (Glucose Assay kit, Cell Biolabs, San Diego, CA). Tissue-specific [1-^{14}C]-2DG-6-phosphate content was

determined via perchloric acid extracted supernatant with Somogyi procedure(18). Glycogen was assessed from [3-^{3}H] glucose incorporated into ethanol-precipitated glycogen in KOH digested tissues(19). Plasma glucose specific activity was calculated from the ratio of plasma glucose radioactivity (dpm) over plasma glucose, multiplied by the ratio of chemical standard evaporated (CSE) to chemical recovery standard (CRS). The [3-^{3}H]-Glucose infusion rate (dpm/kg/min) was then calculated from CSE. Glucose turnover rates (Rd; mg/kg/min) were determined as the ratio of the [3-^{3}H]-Glucose infusion rate and the plasma glucose specific activity of (dpm/mg) at the end of the basal period and during the final 30 min of the clamps. Hepatic glucose production rates (Endo Ra; mg/kg/min) were determined by subtracting the steady-state glucose infusion rate from Rd. Plasma [^{14}C] 2DG specific activity (dpm/mg) was obtained by multiplying the radioactivity disappearance area under the curve of [^{14}C] in plasma samples by CSE/CRS, then divided by the average blood glucose during the clamped time course. Finally, tissue-specific 2DG uptake (Rg; μg glucose/mg tissue/min) was determined as the ratio of the [^{14}C] 2DGp in tissue per tissue weight to plasma [^{14}C] 2DG specific activity. Plasma insulin and C-peptide were measured using mouse ELISA kits (Crystal Chem, Downers Grove, IL).

Primary Hepatocyte Isolation. Primary hepatocytes were prepared from anesthetized lean, chow-fed, male C57Bl/6J mice as previously described(20). Briefly, perfusion buffer (Krebs Ringer with glucose and 0.1 mM EGTA), followed

by digestion buffer (Krebs Ringer with glucose, 1.4 mM $CaCl_2$, 50 µg/mL liberase [Roche, 05401119001]), was infused into the vena cava via peristaltic pump. Hepatocytes were recovered by centrifugation (50xG 3 min, 3 times) and seeded on rat tail type 1 collagen-coated plates in DMEM (10% FBS, 1% Penicillin/Streptomycin) with all experiments conducted <24h post-isolation. Hepatocytes were serum-starved 60 min prior to 2.5 min insulin or glucagon treatment for signaling studies. For glycogen assay hepatocytes were fasted overnight in serum-free, MEMa (1g/L glucose), prior to 2h insulin or IUB288 treatment with [3-^{3}H] glucose.

Immunoblot analyses. Cell extracts were prepared in lysis buffer (20 mm Tris, pH 6.8; 3.8mm DTT, 10% glycerol, 1% SDS, 0.3M PMSF, and HALT protease inhibitor cocktail [Thermo Fisher Scientific, Inc.]), rotated for 15 min at 4°C, and centrifuged for 10 min at 4°C. Equivalent protein amounts were separated by 7.5% SDS-PAGE. Resolved fractions were transferred to PVDF (Bio-Rad Laboratories, Inc., Hercules, CA) and phosphorylation was detected using phosphospecific antibodies to Akt^{473}, Akt^{308}, p44/42 MAPK$^{202/204}$, FoxO1^{24}, GSK-3a/b$^{21/9}$ (Cell Signaling Technology, Danvers, MA) and IRS1^{612} (LifeTechnologies, Frederick, MD). Phosphorylation was normalized by TGX stain-free technology and by immunoblot analysis with anti-AKT, anti-IRS1, FoxO1, and anti-GSK3 (Cell Signaling Technology). Immunoblots were labeled with goat-anti-rabbit horseradish peroxidase-conjugated secondary antibodies and protein bands detected and quantified using Clarity ECL, ChemDoc imaging system, and Image Lab 5.0 software (Bio-Rad Laboratories, Inc., Hercules, CA).

AKT kinase-activity analysis. Kinase analysis was performed in freshly isolated primary hepatocytes following 2.5 minutes of insulin/glucagon treatments using AKT Kinase Assay kit (Cell Signaling #9840). Blots from subsequent immunoblot analysis were imaged using LumoGLO substrate provided in kit and normalized to total protein by TGX stain-free technology.

Statistics. All data are represented as mean and SEM. Statistical significance was determined using unpaired Student's *t*-tests or, where appropriate, one- and two-way analysis of variance (ANOVA) with multiple comparisons Tukey and Sidak post-test, respectively. Statistics were completed using GraphPad Prism version 6.0 for Macintosh (GraphPad Software, San Diego, CA) and significance assigned when $P < 0.05$.

Results

Acute GCGR agonism enhances insulin action and secretion in mice

To interrogate GCGR agonism in glucose metabolism we administered the GCGR-agonist, IUB288(11; 15), to lean, chow-fed C57Bl/6J mice via IP injection (10nmol/kg). IUB288 administration resulted in a rapid rise in glycemia and a subtle increase in plasma insulin (Figure 1a-b), both returning to baseline levels within 60 min. Surprisingly, an ip glucose tolerance test (ipGTT) performed 60min after single injection of IUB288 in lean mice revealed a significant enhancement of glucose tolerance compared to vehicle (Figure 1c). Importantly, this effect was recapitulated by native glucagon (Figure S1a & inset). Consistent with prior observations of GCGR-enhanced glucose-stimulated insulin secretion (GSIS)(21), IUB288 pretreatment (-60min) increased glucose-stimulated insulin levels in response to an intravenous glucose challenge (1 g/kg) (Figure 1d & inset). These data and previous findings (21) suggest that glucagon-stimulated enhancements in GSIS likely contribute to the improved glucose tolerance after GCGR agonism.

Acute GCGR agonism enhances insulin sensitivity in mice

While GCGR-dependent potentiation of GSIS may contribute to enhanced glucose tolerance, this mechanism is unlikely to account for any enhancement of insulin action. To assess the effects of GCGR agonism on insulin-dependent glucose disposal we treated lean mice with IUB288 60 min prior to an insulin tolerance test (ITT, 0.5 U/kg). IUB288 significantly enhanced the response to insulin as determined by both the nadir glucose and the calculated k_g over the initial 30 min period (Figure 1e). To assay endogenous insulin during this test we

measured circulating C-peptide (Figure 1f), and observed that the enhanced insulin action was independent of increased insulin secretion. Importantly, this sensitizing effect was recapitulated by native glucagon during both 0.25U/kg and 0.5U/kg ITTs without an increase in circulating C-peptide (Figure S1b-d) and was similarly observed during co-administration of IUB288 and insulin (Figure S1e).

To assess how long improved insulin action remained evident after GCGR agonism, we increased the pretreatment period (i.e. from 60 to 180min). Even after this extended pretreatment, we observed a beneficial, and dose-dependent effect of IUB288 on insulin action during the ITT (Figure S1f-g). We next assessed insulin sensitivity after GCGR agonism utilizing insulin tolerance tests across a range of insulin doses (0.25-1U/kg). These studies revealed a clear enhancement in insulin action at multiple insulin doses (Figure 2a-d), resulting in increased k_{g30} in both lean (Figure 2e) and DIO mice compared to the vehicle controls (Figure 2f & S2a-d). Similarly, continuous infusion of the short-acting GCGR agonist, ASP28,GLU29-glucagon, 120 min prior to administration of a subthreshold ip insulin bolus (0.25U/kg) increased k_{g20} after GCGR-stimulation (Figure 2g and inset). Importantly, this insulin-sensitizing effect occurred in the absence of prior hyperglycemia (Figure 2g) demonstrating independence from glucagon-induced hyperglycemia.

Glucagon can activate both stimulatory and inhibitory G-protein pathways via the glucagon-like peptide 1 receptor (GLP1R)(22). To investigate potential GLP1R cross-activation we conducted an ipITT with IUB288 pretreatment in GLP1R-deficient (*Glp1r*$^{-/-}$) mice. We found similar insulin-dependent glucose

lowering following IUB288 injection in *Glp1r*$^{-/-}$ mice when compared to their wild type littermates (Figure S3a-b). Likewise, we have reported that GCGR-agonism induces the expression and secretion of FGF21, a known insulin sensitizer(11). However, IUB288 improved insulin sensitivity in global (data not shown) and liver specific, FGF21-deficient (*Fgf21*$^{\Delta liver}$) mice to a similar extent as observed in control mice (Figure S3c-d). Together these data suggest that acute GCGR-agonism enhanced insulin sensitivity independent of GLP1R-signaling or FGF21.

To gain insights into factors contributing to this enhancement of the insulin-dependent glucose metabolism we performed euglycemic clamps. We conducted these clamps (Figure 3a-e) with continuous somatostatin (SST) infusion (1.5 µg/kg/min during the pre-insulin basal condition and 3 µg/kg/min during insulin infusion which was maintained through the termination of the clamp) to control for increased insulin levels observed in IUB288-treated mice (Figure 1). We also included D-[3-^{3}H]-glucose to interrogate hepatic glucose metabolism and [^{14}C]2-deoxyglucose (2DG) to assess tissue-specific glucose uptake. Mice receiving IUB288 initially displayed hyperglycemia (Figure 3a) that was resolved by the second hour of insulin infusion. However, under clamp conditions (t = 90-120), we observed a striking increase in glucose infusion rate (GIR) in IUB288-treated mice (Figure 3b). Importantly, we observed similar GIR potentiation in euglycemic clamp studies conducted without SST (data not shown). Plasma insulin measured at baseline (t=0) and 120 min in our SST-based euglycemic clamp revealed a slight elevation (P=0.0025 [2-way ANOVA], Figure 3c). Importantly, the enhanced GIR observed in IUB288-treated mice was not attributable to differential levels of

circulating insulin (Figure 3c). Glucose disposal (R_d) was likewise increased over vehicle treatment (Figure 3d). Altogether, these data demonstrate that GCGR agonism enhances whole-body insulin sensitivity.

Endogenous glucose production (Ra) in IUB288-treated mice was reduced to a greater extent as compared to vehicle controls ($P<0.0001$ in steady state, Figure 3e and inset), suggesting hepatic insulin sensitivity was enhanced despite the fact that baseline R_a was predictably elevated by IUB288 ($P<0.01$). GCGR agonism significantly reduced liver glycogen content during euglycemic clamp ($P<0.01$, Figure 4a). Likewise, insulin failed to revert the reduction in glycogen promoted by IUB288 in isolated primary hepatocytes (Figure 4b). Hepatocyte glycogen depletion enhances glycogen synthesis and glucose uptake(23), and also stimulates adipocyte lipolysis via a hepatic-CNS-adipose signaling axis(24). To test if depletion of hepatic glycogen stores also acts as a precipitating signal to enhance whole-body insulin sensitivity, we blocked glycogenolysis via the glycogen phosphorylase a/b inhibitor, BAY R3401(25). BAY R3401 was administered 60 min prior to IUB288 treatment (i.e. t=-120) and was sufficient to block 70% of the acute GCGR agonist-stimulated hyperglycemia and to reduce glycemia in lean, chow-fed mice (Figure S4a-b). BAY R3401 pretreatment likewise improved glucose tolerance (Figure S4c) yet did not reduce the incremental area under the curve (iAUC) in these mice (Figure S4d, bars 1 and 3). As in our prior studies, IUB288 pretreatment induced transient hyperglycemia, yet improved glucose tolerance (excursion and iAUC) in vehicle-pretreated mice (Figure S4c-d). However, inhibition of glycogenolysis failed to reduce glucagon-stimulated

enhancement of glucose tolerance (Figure S4d, bars 2 and 4). Altogether, these data suggest that GCGR signaling cooperates with insulin to reduce glucose output independent of its effects on glycogen metabolism.

Unlike in liver, skeletal muscle glycogen was unchanged by IUB288 (Figure 4a). However, we observed elevated [^{14}C]2DG uptake into EDL, quadriceps, gastrocnemius, and soleus (Figure 4c). In contrast to skeletal muscle, glucose uptake was unchanged in WAT (Figure 4c), yet BAT appears to be the primary site of IUB288-stimulated glucose disposal, as [^{14}C]2DG accumulation was increased by 5-fold compared to saline ($p<0.005$, Figure 4d).

Interaction of hepatic glucagon- and insulin-receptor signaling.

Considering high level expression of both GCGR and INSR in liver, we reasoned that hepatic interaction between GCGR and INSR signaling pathways contributed to enhanced insulin sensitivity. We injected chow-fed mice with IUB288 or vehicle 60 min prior to an ip bolus of insulin or vehicle. 10 min later components of the insulin-signaling pathway were analyzed in liver tissue. IUB288 pre-treatment increased the insulin-stimulated phosphorylation at AKT^{Ser473}, but not AKT^{Thr308} (Figure 5a-c), suggesting that GCGR-stimulated enhancement of insulin sensitivity may rely upon a site-specific potentiation of AKT phosphorylation. We next treated isolated hepatocytes with glucagon over a range of insulin concentrations to assess cell autonomous interactions between GCGR and INSR signaling. Phosphorylation of IRS1^{Tyr612} and AKT^{Thr308} by insulin was unaffected by the glucagon co-treatment (Figure 5d,f & S5a-b). Consistent with our *in vivo* studies, glucagon co-treatment directly enhanced insulin-stimulated AKT^{Ser473}

phosphorylation (Figure 5e). We also observed enhanced phosphorylation of the AKT target, Glycogen Synthase Kinase (GSK) 3α/β ($p < 0.01$, Figure S5a-d), but not Forkhead Box protein O1 (FOXO1: Figure S5a-b).

To directly test for enhanced AKT activity, we measured kinase activity of isolated AKT *in vitro*. Phosphorylated-AKT was immunoprecipitated from primary hepatocyte cell lysates prior to incubation with a target peptide. Similar to our observations in liver tissue and isolated hepatocytes, insulin-stimulated AKT activity was significantly enhanced by co-treatment with glucagon (Figure 5g-h). Together these data suggest that GCGR-dependent enhancement of insulin sensitivity is mediated via increased AKT activity.

Analysis of liver samples from clamped mice identified a similar increase in liver AKT^{Ser473} phosphorylation (Figure S6a&e) with reduced phosphorylation at $IRS1^{Tyr612}$, AKT^{Thr308}, and p44/42 $MAPK^{Thr202/Tyr204}$ (Figure S6b-e). Although glucose uptake was enhanced in EDL, AKT^{Ser473} phosphorylation was reduced in this tissue, while AKT^{Thr308} phosphorylation was elevated and phosphorylation at $IRS1^{Tyr612}$ and p44/42 $MAPK^{Thr202/Tyr204}$ were unchanged (Figure S6a-d & f). Finally, in BAT where glucose uptake was most positively regulated; phosphorylation at Akt^{Ser473}, Akt^{Thr308} and p44/42 $MAPK^{Thr202/Tyr204}$ were all enhanced, with a similar trend at $IRS1^{Tyr612}$ (Figure S6a-d & g). Together these data further support a direct and indirect contribution of multiple tissues to the GCGR-dependent enhancement of glucose clearance.

Hepatic glucagon receptors contribute to GCGR-mediated improvements in insulin action.

To investigate the physiological contribution of hepatic GcgRs, we utilized mice deficient for hepatic *Gcgr* (*Gcgr*$^{\Delta liver}$). As previously described(14; 15), these mice exhibit reduced fasting blood glucose (Figure 6a), are refractory to a single provocative IUB288 challenge (Figure 6b) and display dramatically enhanced glucose tolerance (Figure 6c). Unlike in wild type mice, IUB288 had little effect on glucose excursion in *Gcgr*$^{\Delta liver}$ mice (Figure 6c-d). To further dissect the contribution of the hepatic GCGR we challenged mice with an ITT (0.25 U/kg) and observed reduced blood glucose (Figure 6e) and enhanced k_g (Figure 6f) in wild type, but not *Gcgr*$^{\Delta liver}$ mice. Moreover, glucagon co-treatment enhanced insulin-stimulated AKT^{Ser473} phosphorylation in isolated primary hepatocytes from WT, but not *Gcgr*$^{\Delta liver}$ mice (Figure 6g-h), suggesting hepatic GCGR-signaling contributes to insulin-dependent improvement in glycemic control.

Discussion

Data presented here elucidate a novel role for GCGR signaling in insulin sensitivity. As a counterregulatory hormone it is tempting to assume that glucagon opposes all of insulin's actions. However, glucagon secretion and action in the fasting state make it well-suited to potentiate subsequent insulin action. In normal physiology, these data and the previously described prandial glucagon spike(26), suggest that glucagon may act as a preparatory component for the postprandial state. Thus, while chronic GCGR activation impairs glucose tolerance, acute

agonism synergistically enhances insulin action and may also potentiate glucose-dependent insulin secretion.

Mechanistically, we observed that hepatic GCGR-deficient mice were resistant to glucagon-mediated potentiation of insulin action, suggesting that the liver is likely the primary site of action. While these findings highlight the liver (and presumably hepatocytes) as the tissue responsible for this novel GCGR action, a caveat must be acknowledged in this interpretation. Specifically, the *Gcgr*$^{\Delta liver}$ mouse is characterized by supraphysiologic levels of GLP1 and FGF21(27), both potent sensitizers of insulin action, which may contribute to the reported improvement in glucose tolerance(27). In the context of this study, these factors may act to mask any subtle differences between the IUB288- and vehicle-pretreated *Gcgr*$^{\Delta liver}$ mice. Consistent with this observation, we observed a small, but statistically significant difference in glucose excursion between the IUB288- and vehicle-pretreated *Gcgr*$^{\Delta liver}$ mice 30 minutes after glucose challenge. Thus, while the liver is likely the primary site of action, it is possible that the direct potentiation of AKT^{Ser473} phosphorylation and subsequent activity observed in liver may also occur in other tissues.

The acute action of GCGR agonsim to elevate glycemia invokes the possibility that this transient hyperglycemia may trigger insulin secretion and thus improve glucose homeostasis. However, infusion of a short-acting GCGR agonist at doses insufficient to induce hyperglycemia still resulted in a clear and significant increase in insulin action. Likewise, blockade of glycogenolysis (via BAY R3401, Figure S4) ablated GCGR-agonist-induced hyperglycemia, but not IUB288-

enhancement of glucose tolerance. Moreover, our euglycemic clamp protocol included continuous somatostatin infusion to eliminate potential endogenous insulin secretion. We observed glucagon-enhanced insulin actions, including improved glucose tolerance, suppressed hepatic glucose output, and enhanced glucose uptake in the presence of somatostatin. Together we interpret these data to suggest that insulin secretion, downstream of GCGR-agonist-induced hyperglycemia is not the mechanism underlying this enhanced glucose homeostasis.

Although these data cannot exclude a possible cross-activation of other receptors (i.e. GIPR), these insulin-sensitizing effects are clearly GCGR-dependent. Along these lines, hepatic glycogen is known to regulate adipocyte lipolysis via a hepatic-CNS-adipose signaling axis(24). This regulatory pathway is of interest in that it is stimulated by depleted hepatic glycogen levels, similar to what we observe following GCGR agonsim. However, pharmacological blockade of glycogenolysis had no effect on glucagon-stimulated enhancement of glucose tolerance. We interpret these results to conclude that the effects of GCGR-agonsim on glucose tolerance are independent of its effects on glycogen metabolism. While we hypothesize that GCGR and INSR signaling are interacting in a cell autonomous manner at the hepatocyte, insulin also suppresses hepatic glucose production via reduction of circulating free fatty acids(28) (i.e. independent of liver INSR or GCGR signaling). Thus, while the liver is likely the primary site of action, it is possible that the direct potentiation of AKT^{Ser473} phosphorylation and subsequent activity observed in liver may also occur in other tissues. Of particular

note was the enhanced uptake observed in skeletal muscle. Given that GCGR is poorly expressed in skeletal muscle (if at all)(29) this effect is likely mediated indirectly via an alternative endocrine signal and not the direct interactions of GCGR and INSR signaling in these cells.

Importantly, during the preparation of this manuscript, Alonge et al. reported the cooperative intersection of glucagon and insulin signaling in the transcriptional regulation of (*Fgf21*) expression(30). This report, along with our current studies, provide strong evidence for intracellular and cooperative overlap between these two counterregulating hormones. The physiological relevance of Ser^{473} phosphorylation is controversial. However, an emerging view suggests that it precedes Thr^{308} phosphorylation, facilitating activation by PDK1(31). The mechanistic target of rapamycin complex 2 (mTORC2) is responsible for insulin-stimulated AKT^{Ser473} phosphorylation(32). Thus, potentiation of Ser^{473} phosphorylation suggests GCGR agonism may augment this pathway. However, other known mTORC2 targets, paxillin, protein kinase Cα(33), and the serum-and glucocorticoid-induced protein kinase(34), remained unaffected by glucagon (data not shown). These data suggest target-specific activation of the complex following GCGR agonism; or, an inhibition of a phosphatase specifically targeting AKT-Ser^{473}, such as PH domain leucine-rich repeat protein phosphatase(35). Testing these hypotheses will require further experimentation.

The findings described here add to the growing therapeutic attributes of GCGR activation. Specifically, recent reports suggest that co-agonists containing GCGR activity produce superior glucose control as compared to GLP-1, GIP or

thyroid hormones alone(3-5) (36). Likewise, our data may provide mechanistic insight into the paradoxical improvements in the average level of glycemia and a reduction in hyperglycemic events observed in patients utilizing a wearable, bihormonal- (glucagon and insulin) bionic pancreas(37). Thus, these data suggest that GCGR agonism acts both at the level of the liver and pancreas to improve postprandial glycemia. Further, they provide mechanistic insight into the "paradoxical" improvement in glucose homeostasis seen in GCGR-targeted therapeutics.

Acknowledgments:
The project described was supported by the NIH grants 5K01DK098319 and 1R01DK112934 (KMH), R01 DK077975 (DPT), R01 HL128695 (JK), R01 DK082480 (DAS) and P30DK079626. As well as the American Diabetes Association grant 1-13-JF-21 (KMH) and CIHR grants 136942 and 154321 and the Canada Research Chairs Program (DJD).

TK and KMH were responsible for study conception and design, data analyses and interpretation, and drafting the article; TK, CL, CH, SN, DMA, NO, and JC generated experimental data; JK, DS, DJD, RD, and DP-T advised study concept and critical revision of the article. KMH is the guarantor of this work and, as such, had full access to all the data in the study and takes responsibility for the integrity of the data and the accuracy of the data analysis.

We would like to acknowledge Professors David D'Alessio, Stuart Frank, and Anath Shalev for helpful discussion and Ms. Jessica Antipenko, Joyce Sorrel, Sarah Amburgy, Jenna Holland, Chelsea Penny, and Leslie Wilkinson for their technical assistance.

1. Habegger KM, Heppner KM, Geary N, Bartness TJ, DiMarchi R, Tschop MH: The metabolic actions of glucagon revisited. Nature reviews Endocrinology 2010;6:689-697
2. Muller TD, Finan B, Clemmensen C, DiMarchi RD, Tschop MH: The New Biology and Pharmacology of Glucagon. Physiol Rev 2017;97:721-766
3. Day JW, Ottaway N, Patterson JT, Gelfanov V, Smiley D, Gidda J, Findeisen H, Bruemmer D, Drucker DJ, Chaudhary N, Holland J, Hembree J, Abplanalp W, Grant E, Ruehl J, Wilson H, Kirchner H, Lockie SH, Hofmann S, Woods SC, Nogueiras R, Pfluger PT, Perez-Tilve D, DiMarchi R, Tschop MH: A new glucagon and GLP-1 co-agonist eliminates obesity in rodents. Nature chemical biology 2009;5:749-757
4. Clemmensen C, Chabenne J, Finan B, Sullivan L, Fischer K, Kuchler D, Sehrer L, Ograjsek T, Hofmann SM, Schriever SC, Pfluger PT, Pinkstaff J, Tschop MH, Dimarchi R, Muller TD: GLP-1/glucagon coagonism restores leptin responsiveness in obese mice chronically maintained on an obesogenic diet. Diabetes 2014;63:1422-1427
5. Finan B, Yang B, Ottaway N, Smiley DL, Ma T, Clemmensen C, Chabenne J, Zhang L, Habegger KM, Fischer K, Campbell JE, Sandoval D, Seeley RJ, Bleicher K, Uhles S, Riboulet W, Funk J, Hertel C, Belli S, Sebokova E, Conde-Knape K, Konkar A, Drucker DJ, Gelfanov V, Pfluger PT, Muller TD, Perez-Tilve D, DiMarchi RD, Tschop MH: A rationally designed monomeric peptide triagonist corrects obesity and diabetes in rodents. Nature medicine 2015;21:27-36
6. Tan TM, Field BC, McCullough KA, Troke RC, Chambers ES, Salem V, Gonzalez Maffe J, Baynes KC, De Silva A, Viardot A, Alsafi A, Frost GS, Ghatei MA, Bloom SR: Coadministration of glucagon-like peptide-1 during glucagon infusion in humans results in increased energy expenditure and amelioration of hyperglycemia. Diabetes 2013;62:1131-1138
7. Habegger KM, Heppner KM, Amburgy SE, Ottaway N, Holland J, Raver C, Bartley E, Muller TD, Pfluger PT, Berger J, Toure M, Benoit SC, Dimarchi RD, Perez-Tilve D, D'Alessio DA, Seeley RJ, Tschop MH: GLP-1R responsiveness predicts individual gastric bypass efficacy on glucose tolerance in rats. Diabetes 2014;63:505-513
8. Campos GM, Rabl C, Havel PJ, Rao M, Schwarz JM, Schambelan M, Mulligan K: Changes in post-prandial glucose and pancreatic hormones, and steady-state insulin and free fatty acids after gastric bypass surgery. Surgery for obesity and related diseases : official journal of the American Society for Bariatric Surgery 2014;10:1-8
9. Krishna MG, Coker RH, Lacy DB, Zinker BA, Halseth AE, Wasserman DH: Glucagon response to exercise is critical for accelerated hepatic glutamine metabolism and nitrogen disposal. Am J Physiol Endocrinol Metab 2000;279:E638-645
10. Powley TL: The ventromedial hypothalamic syndrome, satiety, and a cephalic phase hypothesis. Psychol Rev 1977;84:89-126
11. Habegger KM, Stemmer K, Cheng C, Muller TD, Heppner KM, Ottaway N, Holland J, Hembree JL, Smiley D, Gelfanov V, Krishna R, Arafat AM, Konkar A, Belli S, Kapps M, Woods SC, Hofmann SM, D'Alessio D, Pfluger PT, Perez-Tilve D, Seeley RJ, Konishi M, Itoh N, Kharitonenkov A, Spranger J, Dimarchi RD, Tschop MH: Fibroblast Growth Factor 21 Mediates Specific Glucagon Actions. Diabetes 2013;
12. Hotta Y, Nakamura H, Konishi M, Murata Y, Takagi H, Matsumura S, Inoue K, Fushiki T, Itoh N: Fibroblast growth factor 21 regulates lipolysis in white adipose

tissue but is not required for ketogenesis and triglyceride clearance in liver. Endocrinology 2009;150:4625-4633
13. Scrocchi LA, Brown TJ, MaClusky N, Brubaker PL, Auerbach AB, Joyner AL, Drucker DJ: Glucose intolerance but normal satiety in mice with a null mutation in the glucagon-like peptide 1 receptor gene. Nature medicine 1996;2:1254-1258
14. Longuet C, Robledo AM, Dean ED, Dai C, Ali S, McGuinness I, de Chavez V, Vuguin PM, Charron MJ, Powers AC, Drucker DJ: Liver-specific disruption of the murine glucagon receptor produces alpha-cell hyperplasia: evidence for a circulating alpha-cell growth factor. Diabetes 2013;62:1196-1205
15. Kim T, Nason S, Holleman C, Pepin M, Wilson L, Berryhill TF, Wende AR, Steele C, Young ME, Barnes S, Drucker DJ, Finan B, DiMarchi R, Perez-Tilve D, Tschoep M, Habegger KM: Glucagon-receptor Signaling Regulates Energy Metabolism Via Hepatic Farnesoid X Receptor and Fibroblast Growth Factor 21. Diabetes 2018;
16. Lockie SH, Heppner KM, Chaudhary N, Chabenne JR, Morgan DA, Veyrat-Durebex C, Ananthakrishnan G, Rohner-Jeanrenaud F, Drucker DJ, DiMarchi R, Rahmouni K, Oldfield BJ, Tschop MH, Perez-Tilve D: Direct control of brown adipose tissue thermogenesis by central nervous system glucagon-like peptide-1 receptor signaling. Diabetes 2012;61:2753-2762
17. Kim T, He L, Johnson MS, Li Y, Zeng L, Ding Y, Long Q, Moore JF, Sharer JD, Nagy TR, Young ME, Wood PA, Yang Q: Carnitine Palmitoyltransferase 1b Deficiency Protects Mice from Diet-Induced Insulin Resistance. J Diabetes Metab 2014;5:361
18. Meszaros K, Lang CH, Bagby GJ, Spitzer JJ: Contribution of different organs to increased glucose consumption after endotoxin administration. The Journal of biological chemistry 1987;262:10965-10970
19. Kim HJ, Higashimori T, Park SY, Choi H, Dong J, Kim YJ, Noh HL, Cho YR, Cline G, Kim YB, Kim JK: Differential effects of interleukin-6 and -10 on skeletal muscle and liver insulin action in vivo. Diabetes 2004;53:1060-1067
20. Li WC, Ralphs KL, Tosh D: Isolation and culture of adult mouse hepatocytes. Methods Mol Biol 2010;633:185-196
21. Huypens P, Ling Z, Pipeleers D, Schuit F: Glucagon receptors on human islet cells contribute to glucose competence of insulin release. Diabetologia 2000;43:1012-1019
22. Weston C, Poyner D, Patel V, Dowell S, Ladds G: Investigating G protein signalling bias at the glucagon-like peptide-1 receptor in yeast. British journal of pharmacology 2014;171:3651-3665
23. Winnick JJ, An Z, Kraft G, Ramnanan CJ, Irimia JM, Smith M, Lautz M, Roach PJ, Cherrington AD: Liver glycogen loading dampens glycogen synthesis seen in response to either hyperinsulinemia or intraportal glucose infusion. Diabetes 2013;62:96-101
24. Izumida Y, Yahagi N, Takeuchi Y, Nishi M, Shikama A, Takarada A, Masuda Y, Kubota M, Matsuzaka T, Nakagawa Y, Iizuka Y, Itaka K, Kataoka K, Shioda S, Niijima A, Yamada T, Katagiri H, Nagai R, Yamada N, Kadowaki T, Shimano H: Glycogen shortage during fasting triggers liver-brain-adipose neurocircuitry to facilitate fat utilization. Nat Commun 2013;4:2316
25. Bergans N, Stalmans W, Goldmann S, Vanstapel F: Molecular mode of inhibition of glycogenolysis in rat liver by the dihydropyridine derivative, BAY R3401:

inhibition and inactivation of glycogen phosphorylase by an activated metabolite. Diabetes 2000;49:1419-1426
26. Geary N: Pancreatic glucagon signals postprandial satiety. Neurosci Biobehav Rev 1990;14:323-338
27. Omar BA, Andersen B, Hald J, Raun K, Nishimura E, Ahren B: Fibroblast growth factor 21 (FGF21) and glucagon-like peptide 1 contribute to diabetes resistance in glucagon receptor-deficient mice. Diabetes 2014;63:101-110
28. Titchenell PM, Chu Q, Monks BR, Birnbaum MJ: Hepatic insulin signalling is dispensable for suppression of glucose output by insulin in vivo. Nat Commun 2015;6:7078
29. Hansen LH, Abrahamsen N, Nishimura E: Glucagon receptor mRNA distribution in rat tissues. Peptides 1995;16:1163-1166
30. Alonge KM, Meares GP, Hillgartner FB: Glucagon and Insulin Cooperatively Stimulate Fibroblast Growth Factor 21 Gene Transcription by Increasing the Expression of Activating Transcription Factor 4. The Journal of biological chemistry 2017;
31. Scheid MP, Marignani PA, Woodgett JR: Multiple phosphoinositide 3-kinase-dependent steps in activation of protein kinase B. Mol Cell Biol 2002;22:6247-6260
32. Sarbassov DD, Guertin DA, Ali SM, Sabatini DM: Phosphorylation and regulation of Akt/PKB by the rictor-mTOR complex. Science 2005;307:1098-1101
33. Sarbassov DD, Ali SM, Kim DH, Guertin DA, Latek RR, Erdjument-Bromage H, Tempst P, Sabatini DM: Rictor, a novel binding partner of mTOR, defines a rapamycin-insensitive and raptor-independent pathway that regulates the cytoskeleton. Curr Biol 2004;14:1296-1302
34. Laplante M, Sabatini DM: mTOR signaling in growth control and disease. Cell 2012;149:274-293
35. Gao T, Furnari F, Newton AC: PHLPP: a phosphatase that directly dephosphorylates Akt, promotes apoptosis, and suppresses tumor growth. Mol Cell 2005;18:13-24
36. Finan B, Clemmensen C, Zhu Z, Stemmer K, Gauthier K, Muller L, De Angelis M, Moreth K, Neff F, Perez-Tilve D, Fischer K, Lutter D, Sanchez-Garrido MA, Liu P, Tuckermann J, Malehmir M, Healy ME, Weber A, Heikenwalder M, Jastroch M, Kleinert M, Jall S, Brandt S, Flamant F, Schramm KW, Biebermann H, Doring Y, Weber C, Habegger KM, Keuper M, Gelfanov V, Liu F, Kohrle J, Rozman J, Fuchs H, Gailus-Durner V, Hrabe de Angelis M, Hofmann SM, Yang B, Tschop MH, DiMarchi R, Muller TD: Chemical Hybridization of Glucagon and Thyroid Hormone Optimizes Therapeutic Impact for Metabolic Disease. Cell 2016;167:843-857 e814
37. Russell SJ, El-Khatib FH, Sinha M, Magyar KL, McKeon K, Goergen LG, Balliro C, Hillard MA, Nathan DM, Damiano ER: Outpatient glycemic control with a bionic pancreas in type 1 diabetes. N Engl J Med 2014;371:313-325

Figure Legends:

Figure 1: GCGR agonism enhances glucose tolerance and insulin secretion. Blood glucose excursion (a) and plasma insulin (b) after single ip challenge of IUB288 in lean, chow-fed C57Bl/6J mice n=7-8 mice/group. Blood glucose (c) during ipGTT with acute IUB288 pretreatment in lean mice (n=27). Plasma insulin (d) and area under the curve (d-inset) during ivGSIS with IUB288 pretreatment (n=7-9). Blood glucose excursion (e) and k_{g30} (e-inset) during ipITT (0.5 U/kg) with IUB288 pretreatment (sc 10nmol/kg) at -60 min (n=17-27). Plasma C-peptide (f) at time 0 and 30 min during 0.5 U/kg ipITT (n=10). See also Figure S1. All data are represented as mean +/- SEM. *p< 0.05, **p< 0.01***, *p*< 0.001, **** *p*< 0.0001 vs vehicle control mice; #*p*<0.05 vs single GCGR agonism.

Figure 2: GCGR agonism enhances insulin action across a range of insulin doses. Blood glucose excursion during ipITT at 0.25 (a), 0.50 (b), 0.75 (c), and 1.0 U/kg insulin (d) in lean, chow-fed mice simultaneous co-treatment with IUB288 (10nmol/kg). Rate of glucose change (kg30, e) calculated from data in panels a - d. Rate of glucose change (kg30, f) of diet-induced, obese mice (data from Figure S2). Blood glucose excursion (g) and kg20 (g, inset) following 120 min of continuous Asp28,Glu29-glucagon treatment via jugular infusion (n=7-9). See also Figure S1 & S2. All data are represented as mean +/- SEM. n=8 mice/group, *p< 0.05, **p< 0.01, ***p< 0.001, ****p< 0.0001.

Figure 3: GCGR agonism enhances hepatic insulin sensitivity during euglycemic-clamp. Blood glucose (a) and glucose infusion rate (b) during labeled, euglycemic-clamp. Plasma insulin (c), glucose disposal (R_d, d), rate of endogenous glucose appearance (Ra, e), and suppression of R_a (e-inset) during labeled, euglycemic-clamp. All data are represented as mean +/- SEM (n = 6-7 mice). See also Figure S5. *p< 0.05, **p< 0.01, ***p< 0.001, **** p< 0.0001 vs baseline time point, # p<0.05, ## p< 0.01, ### p< 0.001, vs vehicle within time points.

Figure 4: GCGR agonism enhances insulin-stimulated non-hepatic glucose uptake during euglycemic-clamp. Liver and quadriceps glycogen content (a) following labeled, euglycemic-clamp. Cellular glycogen levels (b) following 2h IUB288 or IUB288 and insulin co-treatment in primary hepatocytes (n = 3-4 observations). [^{14}C]2DG uptake into extensor digitorum longus, quadriceps, gastrocnemius, soleus, epididymal white adipose tissue (c), and brown adipose tissue (d). All data are represented as mean +/- SEM (n = 6-7 mice). See also Figure S5. *p< 0.05, *** p< 0.001, **** p< 0.0001.

Figure 5: Convergence of GCGR and Insulin signaling at AKT. Immunoblot analysis of liver AKT phosphorylation in response to insulin and IUB288. IUB288 (10nmol/kg) injected 60 min prior to 10 min insulin challenge. Representative images of phosphorylation on residues Ser^{473} and Thr^{308} (a) and densitometric quantification (b & c) of 7-8 mice/group. Immunoblot analysis of hepatocyte insulin

signaling in response to insulin and glucagon co-treatment (d - f). Representative images (d) and densitometric quantification (e & f) of 6 independent/observations. Kinase activity analysis of hepatocyte AKT in response to insulin and IUB288 co-treatment. Representative image of *in vitro* phosphorylation of exogenous AKT substrate (GSK3, g). Densitometric quantification (h) of 4 independent observations. See also Figure S6. All data are represented as mean +/- SEM. *p< 0.05 vs baseline time point; # p<0.05, ## *p*< 0.01 vs vehicle within time points.

Figure 6: Hepatic Receptors Contribute to GCGR-mediated improvements in insulin action. Fasting blood glucose (a) and ip IUB288-stimulated blood glucose excursion (b) in WT and *Gcgr*$^{\Delta liver}$ mice. GTT (c) and area under the curve analysis (d) in WT and *Gcgr*$^{\Delta liver}$ mice with IUB288 pretreatment. Insulin Tolerance Test (e) and k_{g15} analysis (f) in WT and *Gcgr*$^{\Delta liver}$ mice with 60min IUB288 pretreatment administered sc at 10nmol/kg throughout. Immunoblot analysis of AKT phosphorylation in response to insulin and glucagon co-treatment in hepatocytes isolated from WT or *Gcgr*$^{\Delta liver}$ mice (g-h). All data are represented as mean +/- SEM. *p< 0.05, **p< 0.01, ***p< 0.001, **** p< 0.0001 WT vehicle vs WT IUB288; $^{\#}$p< 0.05 GcgR$^{\Delta liver}$ vehicle vs GcgR$^{\Delta liver}$ IUB288. $^{\&\&}$p< 0.01 WT insulin vs WT insulin+IUB288. $^{\$\$\$\$}$ p< 0.0001 WT insulin+IUB288 vs *Gcgr*$^{\Delta liver}$ insulin+IUB288

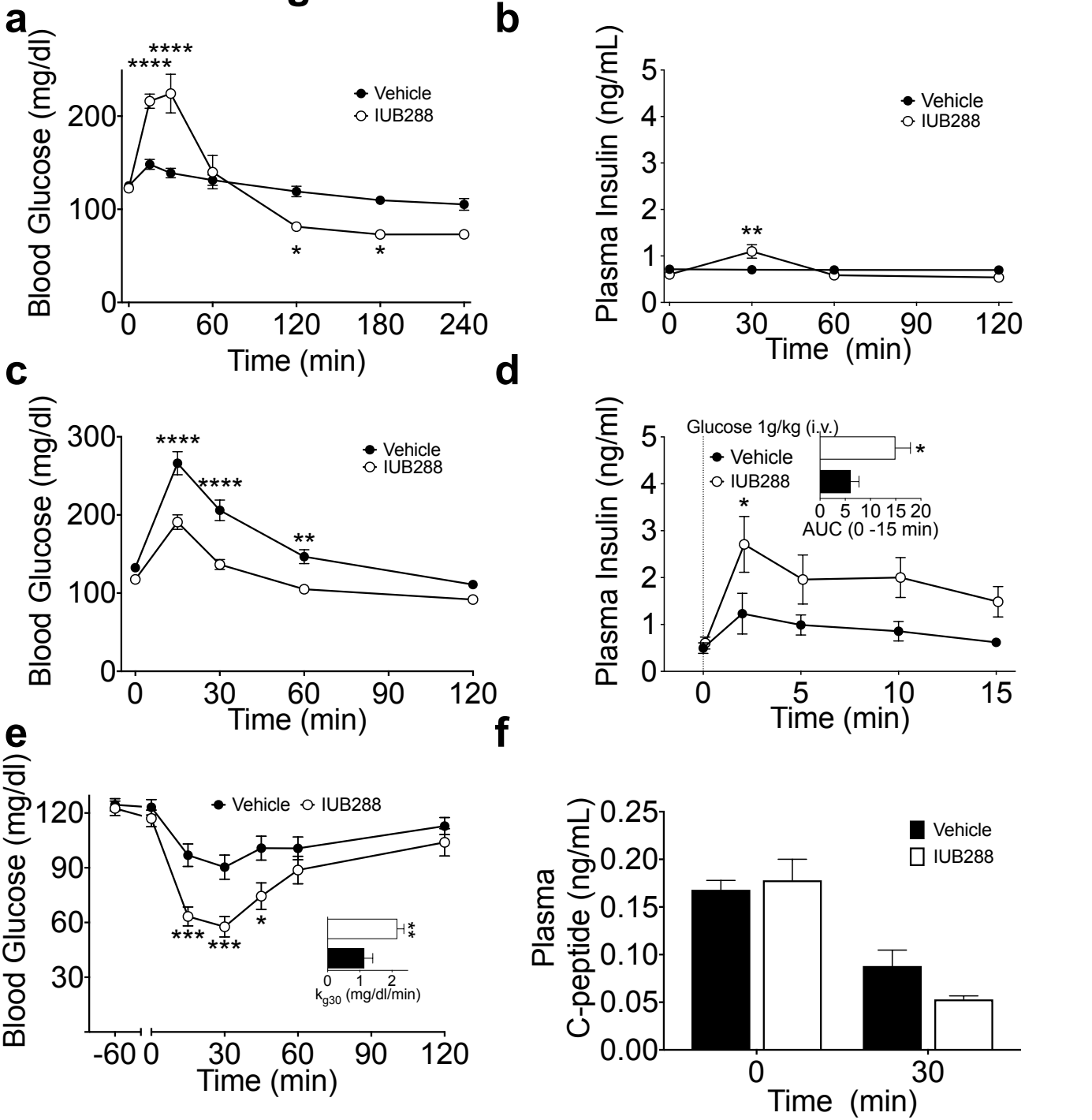
a
Blood Glucose (mg/dl)
Time (min)
Vehicle
IUB288
b
Plasma Insulin (ng/mL)
Time (min)
Vehicle
IUB288
c
Blood Glucose (mg/dl)
Time (min)
Vehicle
IUB288
d
Plasma Insulin (ng/ml)
Time (min)
Glucose 1g/kg (i.v.)
Vehicle
IUB288
AUC (0 -15 min)
e
Blood Glucose (mg/dl)
Time (min)
Vehicle
IUB288
k g30 (mg/dl/min)
f
Plasma C-peptide (ng/mL)
Time (min)
Vehicle
IUB288

Figure 2

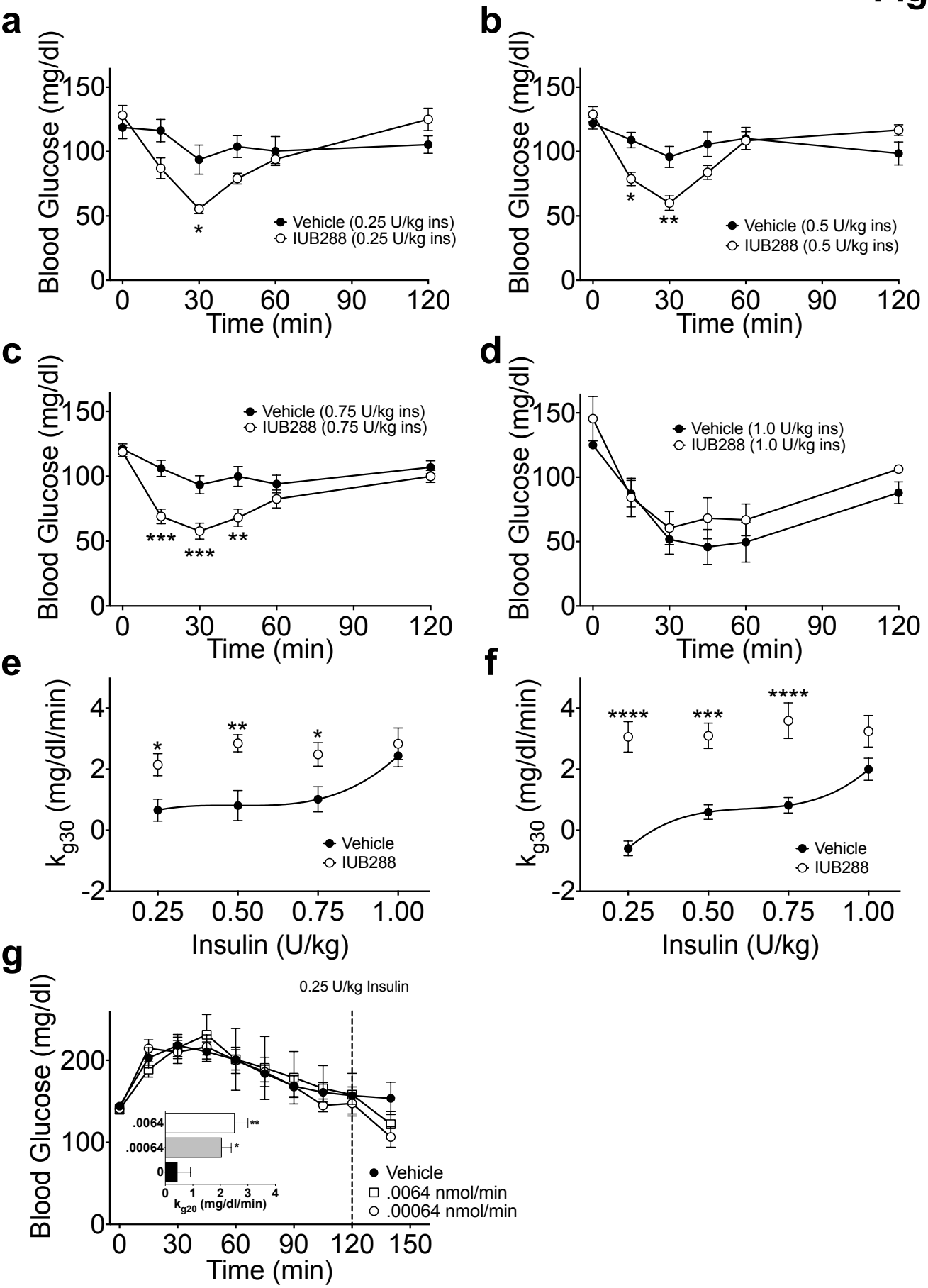
a
Blood Glucose (mg/dl)
Time (min)
Vehicle (0.25 U/kg ins)
IUB288 (0.25 U/kg ins)
b
Vehicle (0.5 U/kg ins)
IUB288 (0.5 U/kg ins)
c
Vehicle (0.75 U/kg ins)
IUB288 (0.75 U/kg ins)
d
Vehicle (1.0 U/kg ins)
IUB288 (1.0 U/kg ins)
e
k_{g30} (mg/dl/min)
Insulin (U/kg)
Vehicle
IUB288
f
g
0.25 U/kg Insulin
.0064
.00064
0
k_{g20} (mg/dl/min)
Vehicle
.0064 nmol/min
.00064 nmol/min

Figure 3

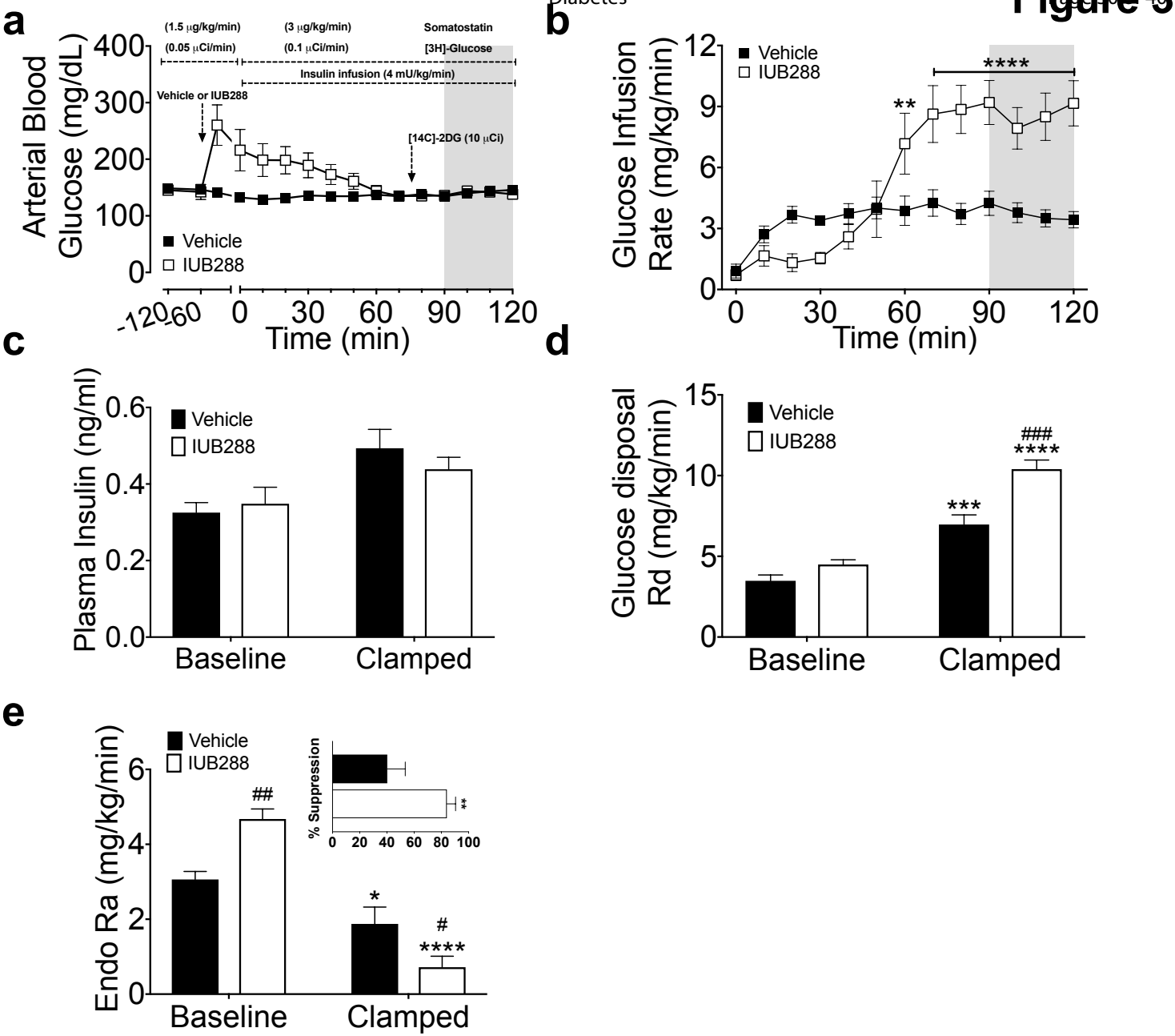
a
(1.5 μg/kg/min)
(0.05 μCi/min)
(3 μg/kg/min)
(0.1 μCi/min)
Somatostatin
[3H]-Glucose
Insulin infusion (4 mU/kg/min)
Vehicle or IUB288
[14C]-2DG (10 μCi)
Arterial Blood Glucose (mg/dL)
Vehicle
IUB288
Time (min)
b
Glucose Infusion Rate (mg/kg/min)
Vehicle
IUB288
**
****
Time (min)
c
Plasma Insulin (ng/ml)
Vehicle
IUB288
Baseline
Clamped
d
Glucose disposal Rd (mg/kg/min)
Vehicle
IUB288
***
###
****
Baseline
Clamped
e
Endo Ra (mg/kg/min)
Vehicle
IUB288
##
% Suppression
**
*
#
****
Baseline
Clamped

Figure 4

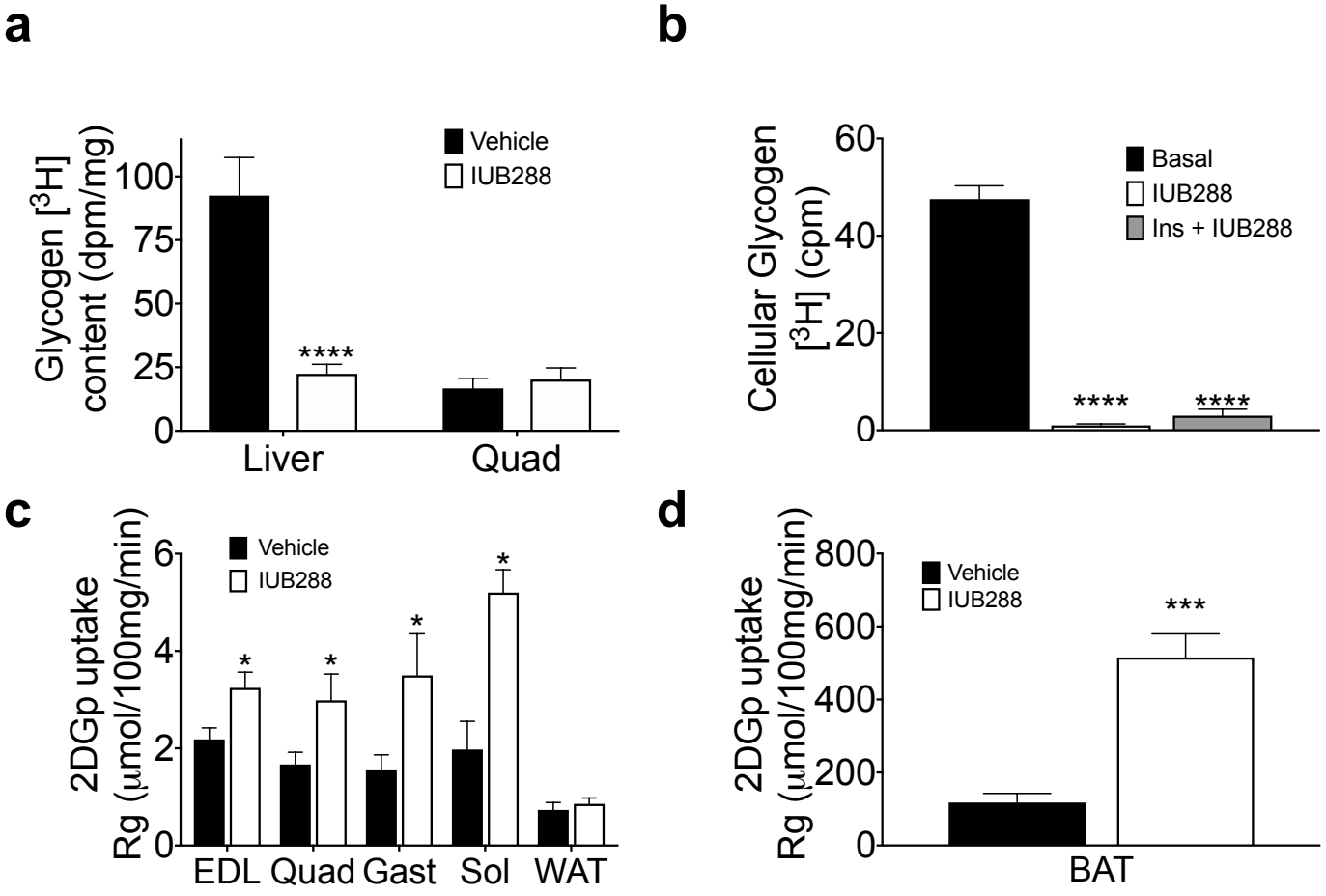
a
Glycogen [3H] content (dpm/mg)
100
75
50
25
0
Vehicle
IUB288
****
Liver
Quad
b
Cellular Glycogen [3H] (cpm)
60
40
20
0
Basal
IUB288
Ins + IUB288
****
****
c
2DGp uptake Rg (µmol/100mg/min)
6
4
2
0
Vehicle
IUB288
*
*
*
*
EDL
Quad
Gast
Sol
WAT
d
2DGp uptake Rg (µmol/100mg/min)
800
600
400
200
0
Vehicle
IUB288
***
BAT

Figure 5

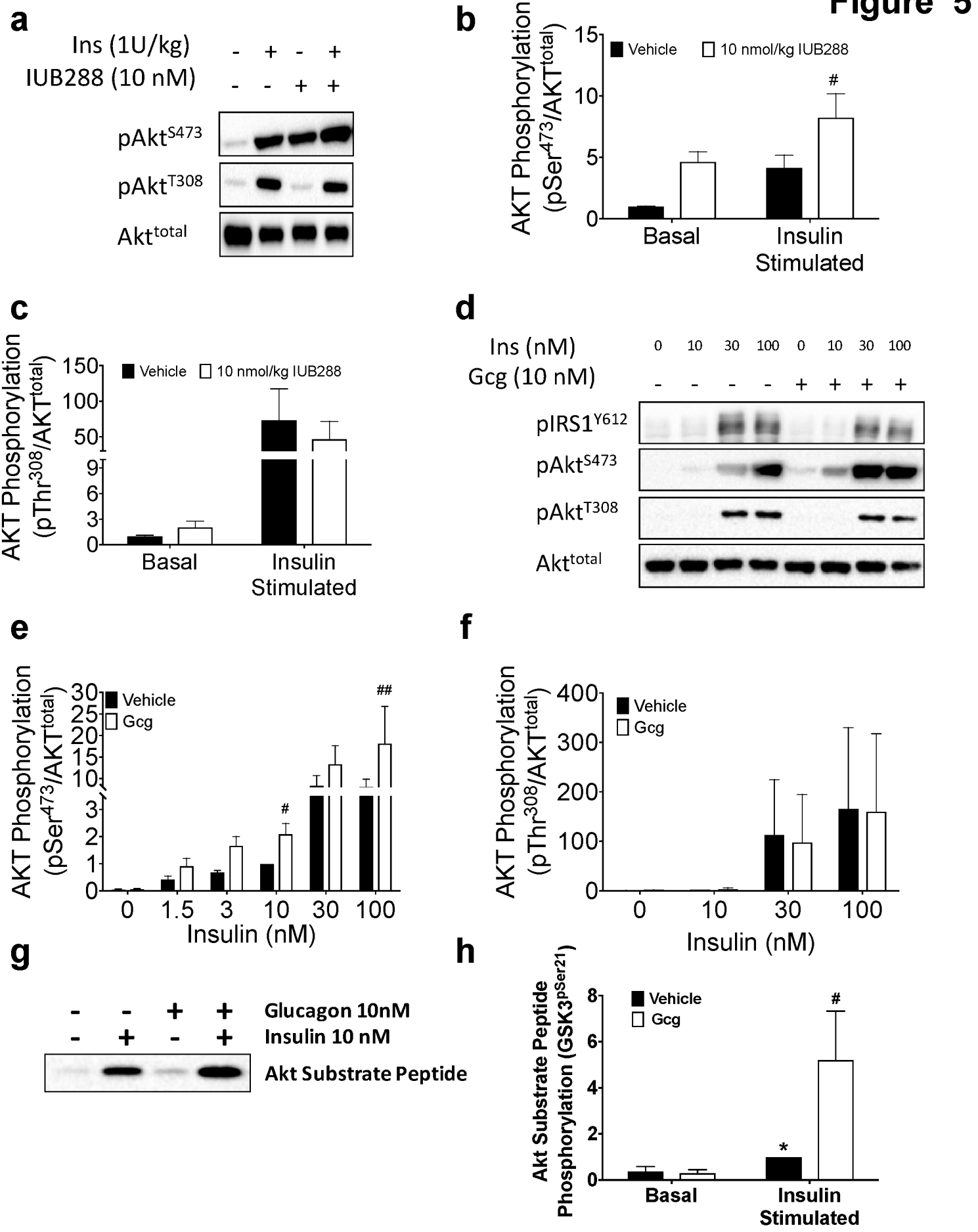
a
Ins (1U/kg) - + - +
IUB288 (10 nM) - - + +
pAkt^S473
pAkt^T308
Akt^total
b
AKT Phosphorylation (pSer^473/AKT^total)
Vehicle
10 nmol/kg IUB288
#
Basal
Insulin Stimulated
c
AKT Phosphorylation (pThr^308/AKT^total)
Vehicle
10 nmol/kg IUB288
Basal
Insulin Stimulated
d
Ins (nM) 0 10 30 100 0 10 30 100
Gcg (10 nM) - - - - + + + +
pIRS1^Y612
pAkt^S473
pAkt^T308
Akt^total
e
AKT Phosphorylation (pSer^473/AKT^total)
Vehicle
Gcg
#
##
Insulin (nM)
f
AKT Phosphorylation (pThr^308/AKT^total)
Vehicle
Gcg
Insulin (nM)
g
Glucagon 10nM
Insulin 10 nM
Akt Substrate Peptide
h
Akt Substrate Peptide Phosphorylation (GSK3^pSer21)
Vehicle
Gcg
*
#
Basal
Insulin Stimulated

Figure 6

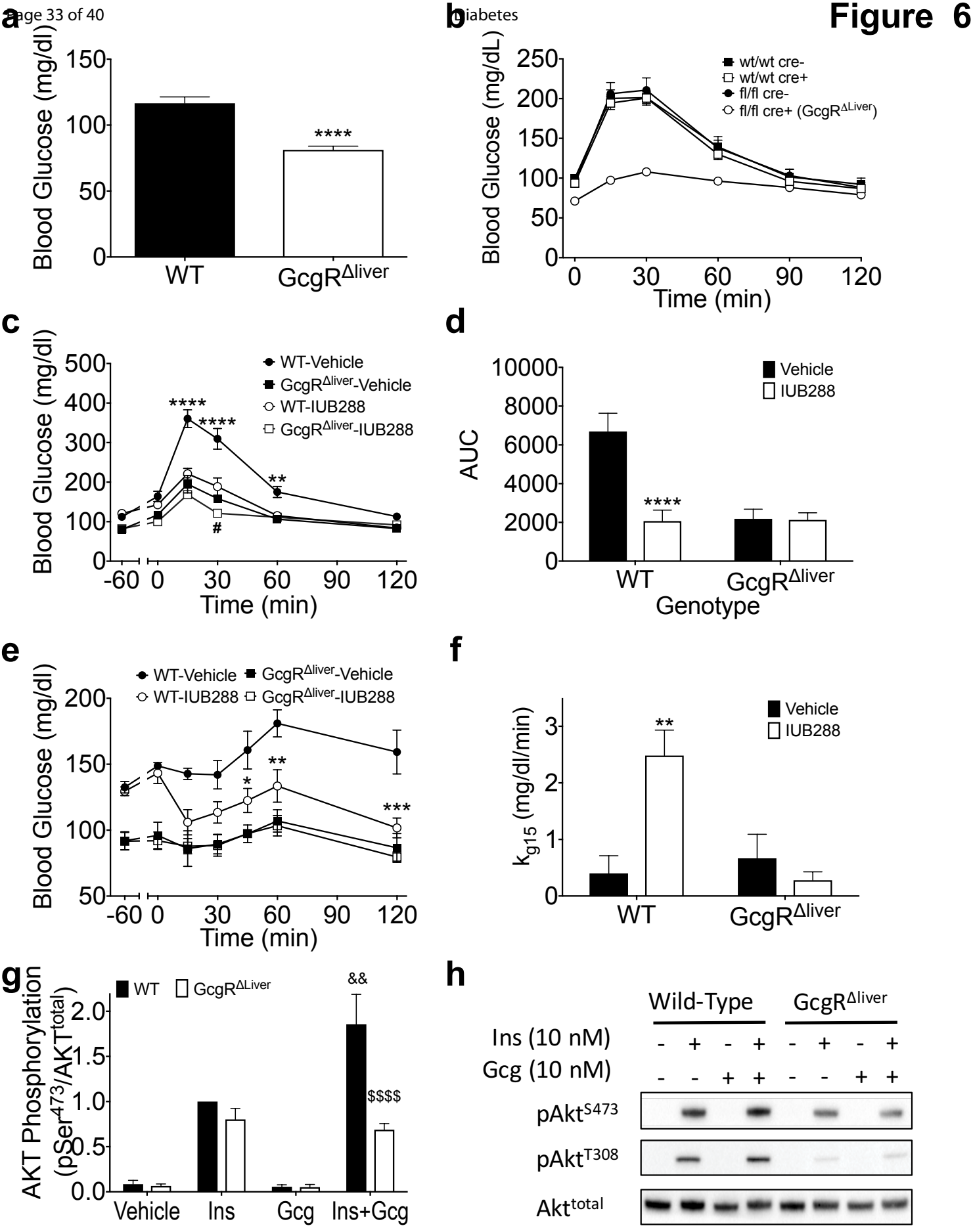
a
Blood Glucose (mg/dl)
150
100
50
0
****
WT
GcgR^ΔLiver
b
Blood Glucose (mg/dL)
250
200
150
100
50
0
wt/wt cre-
wt/wt cre+
fl/fl cre-
fl/fl cre+ (GcgR^ΔLiver)
0
30
60
90
120
Time (min)
c
Blood Glucose (mg/dl)
500
400
300
200
100
0
WT-Vehicle
GcgR^ΔLiver-Vehicle
WT-IUB288
GcgR^ΔLiver-IUB288
****
****
**
#
-60
0
30
60
90
120
Time (min)
d
AUC
10000
8000
6000
4000
2000
0
Vehicle
IUB288
****
WT
GcgR^ΔLiver
Genotype
e
Blood Glucose (mg/dl)
200
150
100
50
WT-Vehicle
GcgR^ΔLiver-Vehicle
WT-IUB288
GcgR^ΔLiver-IUB288
*
**
***
-60
0
30
60
90
120
Time (min)
f
k_g15 (mg/dl/min)
3
2
1
0
Vehicle
IUB288
**
WT
GcgR^ΔLiver
g
AKT Phosphorylation (pSer^473/AKT^total)
2.0
1.5
1.0
0.5
0.0
WT
GcgR^ΔLiver
&&
$$$$
Vehicle
Ins
Gcg
Ins+Gcg
h
Wild-Type
GcgR^ΔLiver
Ins (10 nM)
Gcg (10 nM)
- + - + - + - +
- - + + - - + +
pAkt^S473
pAkt^T308
Akt^total

Supplemental Figure Legends:

Figure S1: The beneficial effects of acute GCGR agonism are Glucagon-specific. Glucose Tolerance Test (GTT) (a) and area under the curve analysis (a-inset) in C57Bl/6J mice with or without 60 min native glucagon (10nmol/kg) pretreatment (n=6). 0.25U/kg Insulin Tolerance Test (ITT) and kg15 (b), 0.5U/kg ITT and kg30 (c), and plasma C-peptide (d) during 0.5U/kg ITT in C57Bl/6J mice with or without 60 min glucagon (10nmol/kg) pretreatment (n=14-16). ip (0.25 U/kg) after IUB288 (10nmol/kg) and insulin co-treatment (e). ITT (0.25 U/kg) (f) and blood glucose nadir (g) in lean, chow-fed mice pretreated with various doses of IUB288 (0, 0.3, 1, 3, and 10nmol/kg) for 180 min (n=7-9). All data are represented as mean +/- SEM. *p< 0.05, **p< 0.01, ***p< 0.001,

Figure S2: Acute GcgR agonism enhances insulin action in obese mice. Insulin Tolerance Test (ITT) at 0.25 (a), 0.50 (b), 0.75 (c), and 1.0 U/kg (d) insulin in DIO mice with single injection of IUB288 (10nmol/kg) at -60 min. All data are represented as mean +/- SEM. n=8 mice/group.

Figure S3: The beneficial effects of acute GcgR agonism are GLP1R and FGF21 independent. Insulin Tolerance Test (ITT) (0.25U/kg insulin) (a) and rate of glucose change (kg30, b) of Control and GLP1-R deficient mice with or without 60 min ip IUB288 (10nmol/kg) pretreatment. ITT (0.25U/kg insulin) (c) and rate of glucose change (kg15, d) of Control and *Fgf21*$^{\Delta Liver}$ mice with or without ip 60 min IUB288 (10nmol/kg)

pretreatment. All data are represented as mean +/- SEM. *p< 0.05, **p< 0.01, ***p< 0.001 vs Control vehicle within time points, $^{\#}$p< 0.05 vs *Fgf21*$^{\Delta liver}$ vehicle within time points

Figure S4: The beneficial effects of acute GcgR agonism are independent of glycogen depletion. Blood glucose excursion (a) and 15min change (b) in response to GcgR agonsim (10nmol/kg IUB288) in the presence or absence of glycogen phosphorylase a/b inhibitor (10mg/kg BAY R3401) in C57Bl/6J mice. GTT (2g/kg) (c) and area under the curve analysis (d) following ip glucose challenge IUB288- and BAY R3401-treated and control mice (n=6). All data are represented as mean +/- SEM, **p< 0.01, ***p< 0.001

Figure S5: GcgR agonism enhances insulin action at GSK3. Immunoblot analysis of hepatocyte insulin signaling in response to low- (a) and high- (b) dose insulin and glucagon co-treatment. Representative images of 6 independent/observations. Immunoblot analysis of GSK3α/β phosphorylation (c & d) in response to insulin and glucagon co-treatment in isolated hepatocytes (see Figure 3d). All data are represented as mean +/- SEM of 4 independent/observations. *p< 0.05, **p< 0.01, ***p< 0.001.

Figure S6: Insulin signaling during labeled, euglycemic clamp. Immunoblot analysis in liver, EDL, and BAT from clamped mice (Figures 3-4). Densitometric quantification (a-d) and representative images (e-g) of insulin signaling pathway components in 6-7 mice/group. *p< 0.05, **p< 0.01.

Figure S1: Related to Figure 1

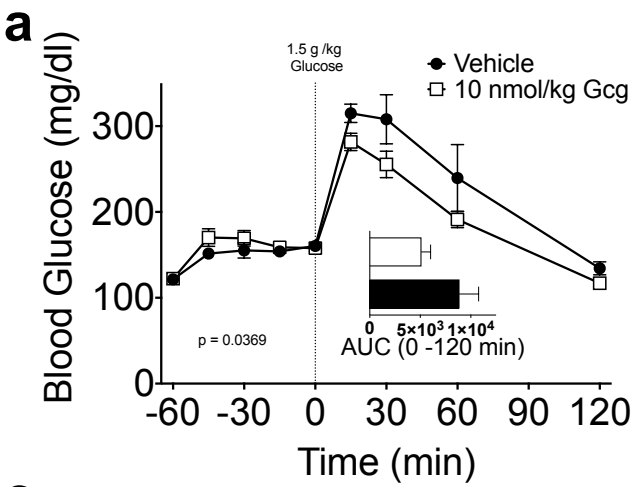

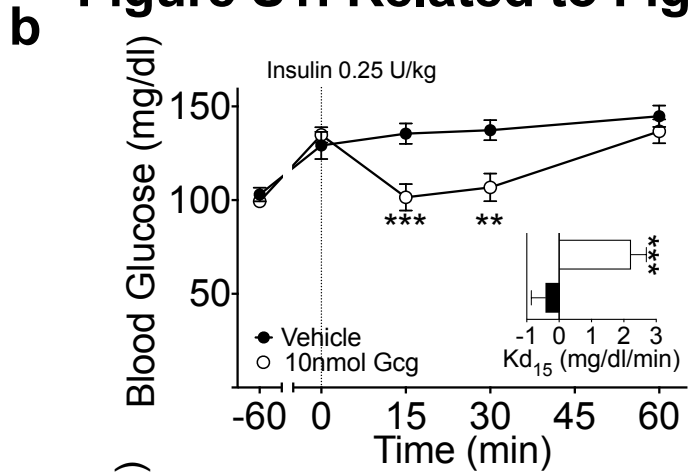

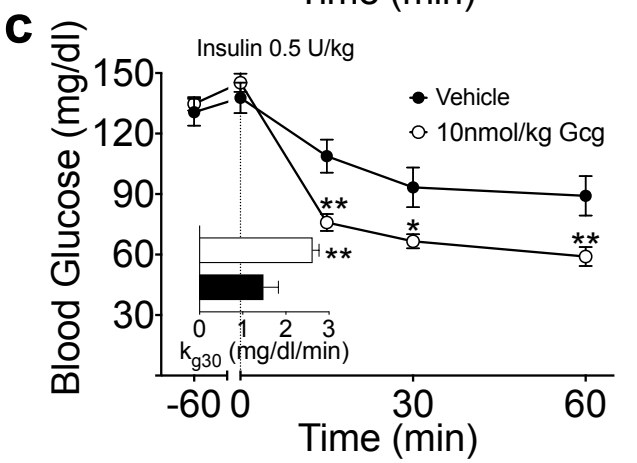

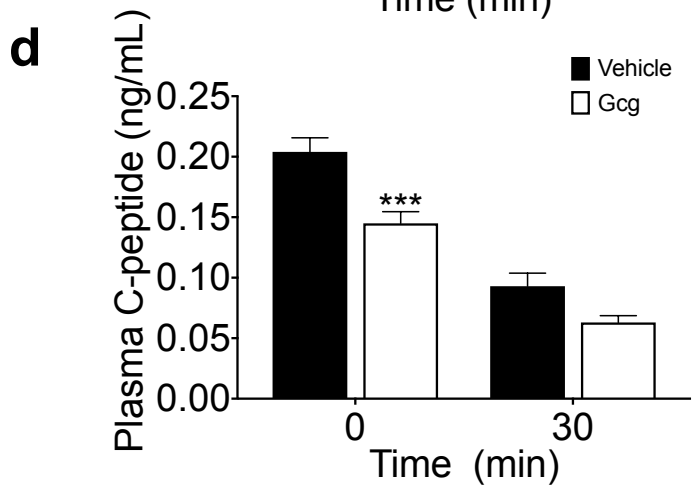

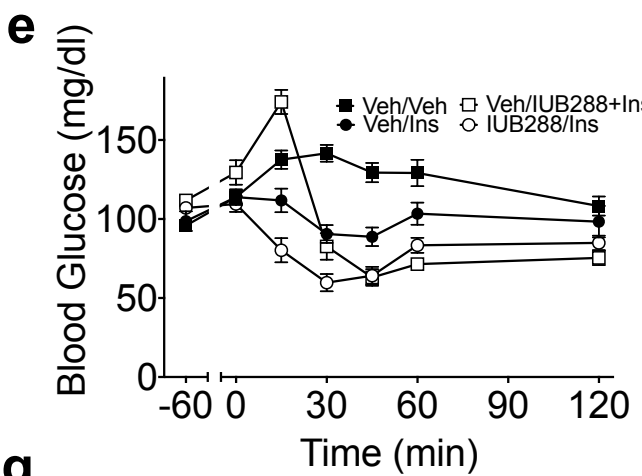

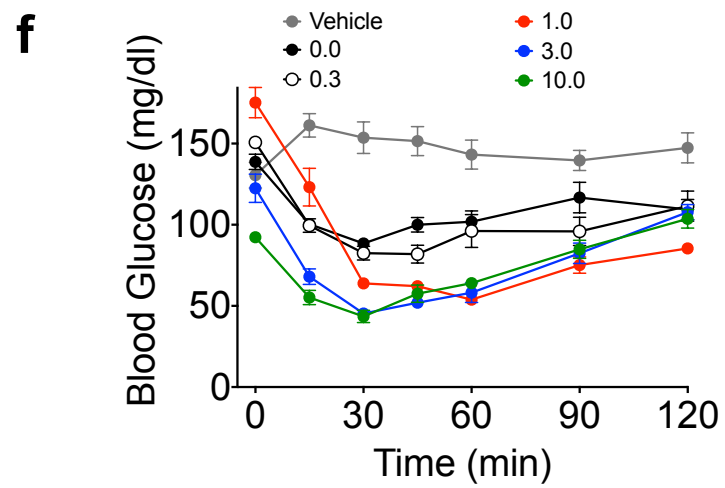

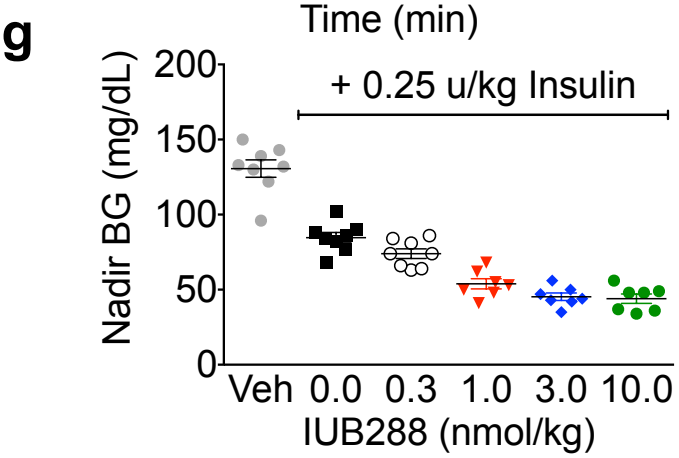

Figure S2: Related to Figure 2

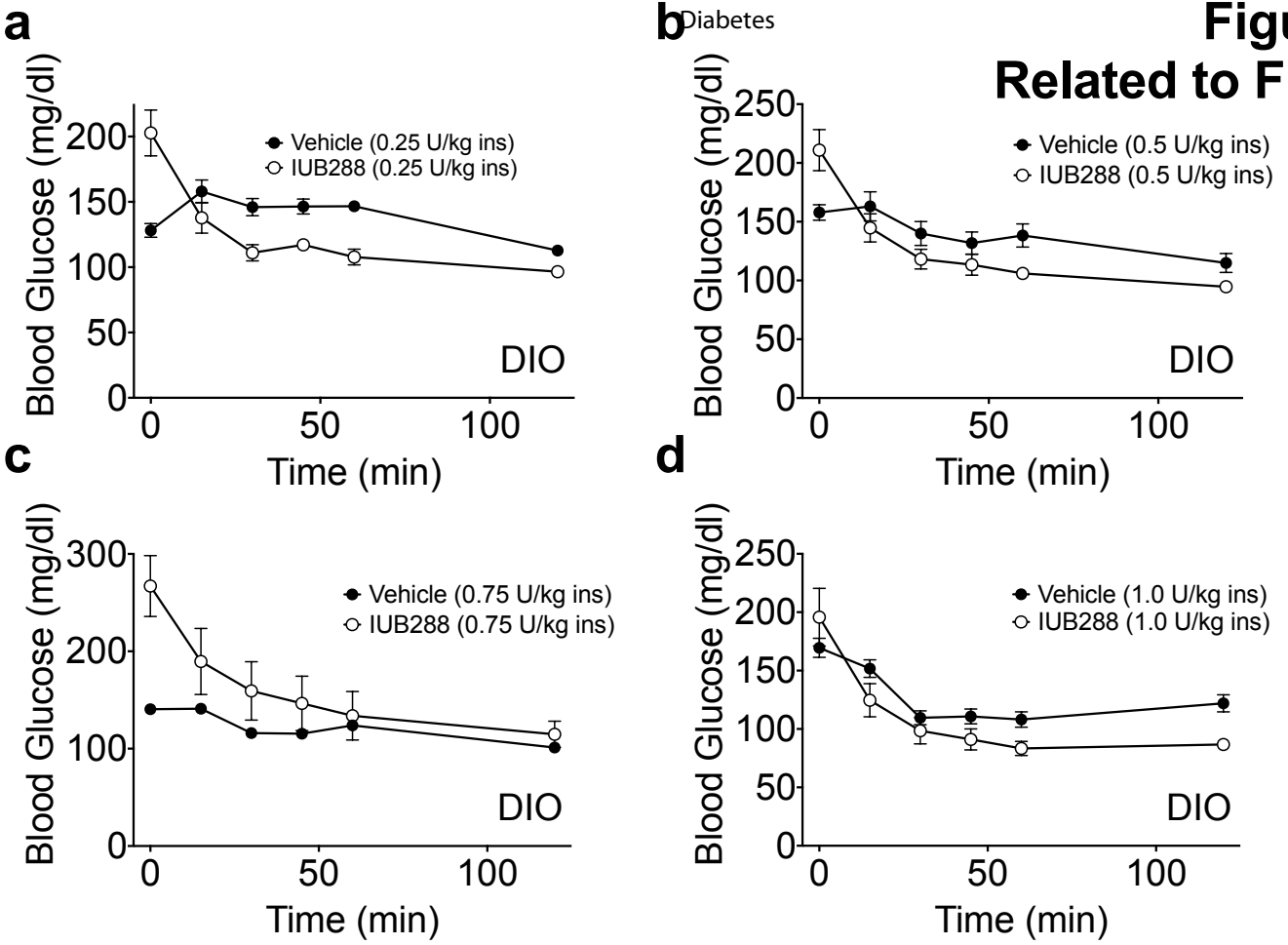

Figure S3: Related to Figure 2

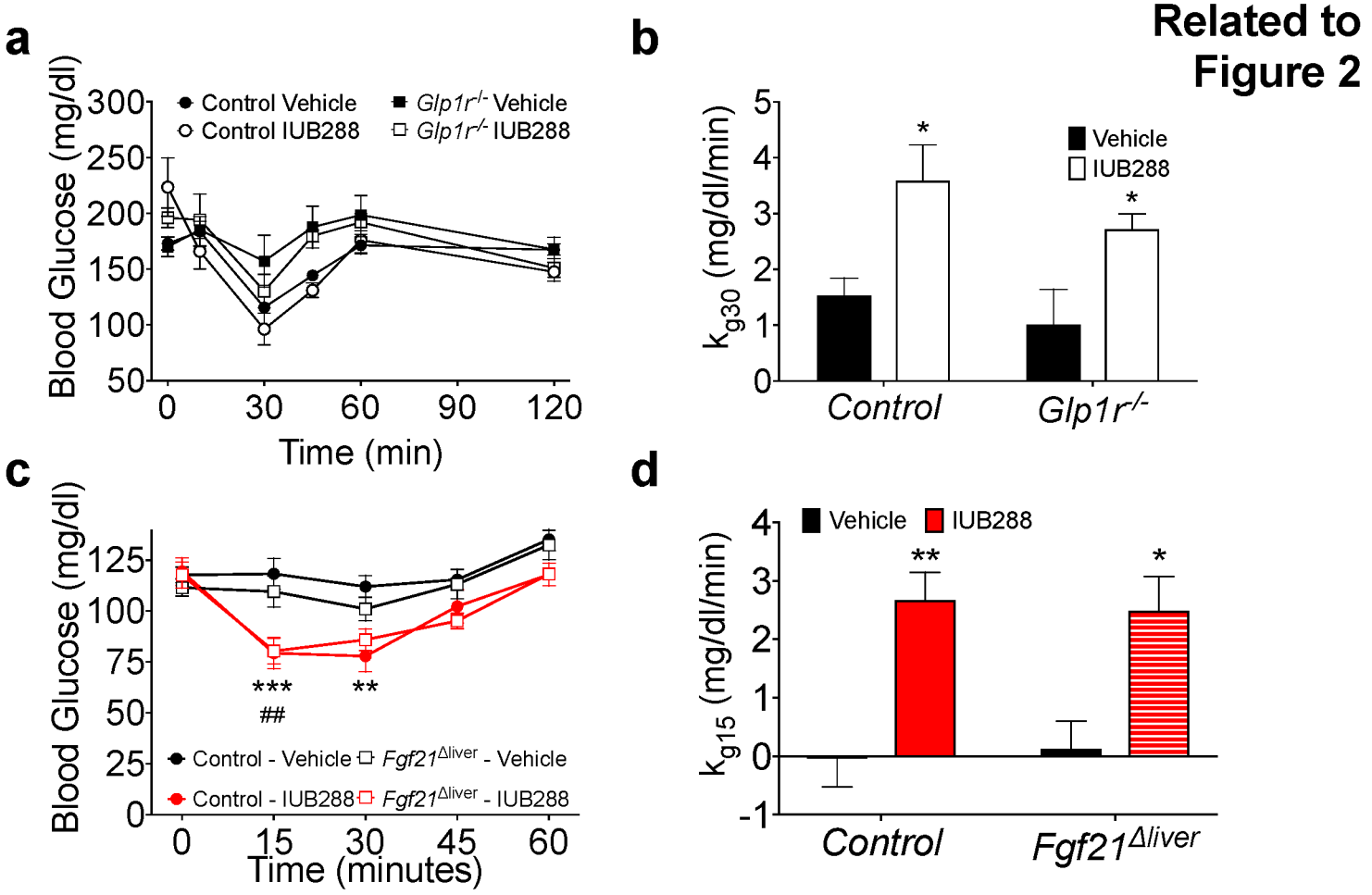

Figure S4: Related to Figure 4